Structure of Biomolecular Condensates from Dissipative Particle Dynamics Simulations

Julian C. Shillcock[1]*, Maelick Brochut[2], Etienne Chénais[2], John H. Ipsen[3]

[1] Laboratory of Molecular and Chemical Biology of Neurodegeneration, Ecole polytechnique fédérale de Lausanne, CH-1015 Lausanne, Switzerland

[2] Brain Mind Institute, Ecole polytechnique fédérale de Lausanne, CH-1015 Lausanne, Switzerland

[3] Dept. of Physics, Chemistry and Pharmacy, University of Southern Denmark, Campusvej 55, DK-5230 Odense M, Denmark

* Correspondence: julian.shillcock@epfl.ch

ABSTRACT

Biomolecular condensates are compositionally-diverse organelles that reversibly assemble in the cytoplasm or nucleoplasm to localize cellular functions. They form by liquid-liquid phase separation and have no bounding lipid membrane. Experiments have shown that biomolecular condensates have a wide range of functions, and loss of cellular control is associated with chronic neurodegenerative diseases. Their main constituents are intrinsically-disordered proteins that are conformationally flexible and possess weak binding sites for proteins or RNA. Although the composition of many experimental condensates is increasingly clear, the quantitative connection between their structure and the molecular properties of their constituent proteins is still obscure. We use coarse-grained molecular simulations to explore the phase behaviour of a model biomolecular condensate and its dependence on its constituent intrinsically-disordered proteins. The proteins are represented as semi-flexible polymers with attractive end-caps. They spontaneously condense into fluid networks in which

their end-caps reversibly bind at junctions. The spatial separation of the junctions scales with the polymer backbone length as a self-avoiding random walk. The network stability and structure are more sensitive to the separation of the end-caps than their affinity. This sensitivity to the binding site separation suggests that post-translational modifications or interactions with other proteins that modify the conformational fluctuations of a disordered protein will regulate its transition into a condensed phase. Additional proteins will be recruited only if their conformational fluctuations allow them to fluctuate between the existing junctions of the network. Cells may use this sensitivity to regulate assembly and composition of biomolecular condensates, and it provides a promising route towards therapeutic interventions

KEYWORDS: Biomolecular condensate, Membraneless organelle, Liquid-Liquid phase separation, Phase transition, Intrinsically disordered protein, Dissipative Particle Dynamics, Coarse-grained simulation.

Biomolecular condensates (BC) are compositionally-diverse assemblies of protein in the cellular cytoplasm and nucleoplasm that form by liquid-liquid phase separation (LLPS) of their constituents from their environment.[1] They have multiple roles in the cell[2] including regulation,[3] sequestering RNA stalled in translation during stress,[4] cellular signalling networks,[5-7] and neuronal synapses in the brain.[8] They have also been shown to exert mechanical forces that restructure chromatin.[9] Although they lack a protective membrane barrier, their assembly and composition are tightly regulated by the cell, and loss of control is associated with chronic diseases including Alzheimer's, Parkinson's and Huntington's disease.[10] Their constituents are intrinsically-disordered proteins (IDP) that have little or no secondary structure, often contain repeated short sequences of amino acids (so-called *low-complexity* domains), and no conserved sequence similarity.[11, 12] IDPs interact via weak, multivalent binding sites by which they transiently bind to other proteins or RNA and induce phase

separation.[13] They also have no lowest-energy, folded state but instead exhibit a large ensemble of conformational states in equilibrium.[14, 15] It is not yet understood how the structure of biomolecular condensates arises from their constituent IDPs, nor why they transform into pathological rigid states in disease and ageing.[16] Because the large conformational fluctuations, and weak interactions of IDPs underpin their ability to undergo liquid-liquid phase separation, it may be fruitful to explore how far the properties of their condensed phase can be derived from a physical chemical model of IDPs as weakly-associating, semi-flexible polymers. The theoretical insights obtained may illuminate the internal structure of BCs and provide insight into their pathological transformations.

A wide range of experimental techniques have been used to probe the physical properties of BCs.[17] They present special challenges due to the tendency of their constituent IDPs to aggregate at low concentrations and their susceptibility to post-translational modifications.[18] Fused in Sarcoma (FUS) is an IDP implicated in several chronic neurological disorders including Amyotrophic Lateral Sclerosis and frontotemporal lobar dementia.[19] Patel *et al.* have used cryoelectron microscopy to show that FUS droplets are amorphous and lack ordered structures.[4] Burke *et al.* used solution NMR spectroscopy to show that the low-complexity domain of monomeric FUS (FUS LC) lacks any secondary structure and this disordered state is retained within phase-separated droplets.[20] They also found that while translational diffusion of FUS LC within droplets is dramatically slowed, its local motion and conformational fluctuations are retained. They inferred that the FUS LC chain forms transient intermolecular contacts that are sufficiently short-lived that they are still able to reorient. Recent experiments have confirmed that FUS LC within phase separated droplets lacks secondary structure, and also showed that distinct types of multivalent binding (hydrogen bonding, hydrophobic and π/sp2 interactions) contribute to LLPS of the FUS LC.[19] Similar structural disorder has been observed in the condensed phase of

other IDPs. Brady *et al.* used solution NMR to show that the protein Ddx4 inside BCs is flexible and disordered although its diffusion constant is 100-fold smaller than in bulk solution.[21] Wei *et al.* used ultrafast scanning Fluorescence Correlation Spectroscopy (FCS) to show that LAF-1 proteins inside P granules in C Elegans embryos form a surprisingly dilute phase[22] although it is 50 times more concentrated than the protein concentration in the bulk phase. They find that the condensed protein network has a characteristic mesh size of 3 – 8 nm. Cryo-Electron Tomography of Sup35, a yeast prion protein, shows that as a response to cellular stress it forms a BC that is a porous network with a mesh spacing around 10 nm.[23] Non-biological peptides also phase separate into condensed droplets with an unexpectedly low internal density as a function of temperature and an inert crowding agent.[24]

The picture emerging from these experiments is that the internal structure of BCs resembles a porous network in which the constituent IDPs transiently bind to each other but are otherwise disordered. Intuitively, it is unclear why dispersed IDPs should condense at low concentrations when it should be thermodynamically more favourable for them to remain dispersed and maximise their entropy. Classical polymer theory (regular solution or Flory Huggins theory) predicts that a mixture of dissimilar polymers phase separates when their tendency to mix driven by their translational entropy is overcome by their enthalpic drive to demix.[25] This theory has been applied to the demixing of IDPs,[14] but its relevance is questionable. IDPs are typically water-soluble proteins that lack a strong demixing tendency, and the theory does not explain the role of protein multivalency,[26] the low internal concentration inside the condensed phase,[22] nor their very low surface tension.[27] Consequently, interest has turned to computer simulations to reveal the phase behaviour of IDPs.[28]

Atomistic Molecular Dynamics simulations have been used to study the conformations of peptides,[29] and the disease-related proteins Huntingtin,[30] α-

synuclein,[31] tau,[32] as well as the assembly of IDPs into oligomers.[33] But typical atomistic force fields have been optimized for folded proteins and must be modified in order to faithfully recreate the conformational flexibility of IDPs such as α-synuclein.[34] Even then, the secondary structure of a simulated protein can be more strongly affected by changing the force field than changing the entire peptide sequence.[29] Because IDPs with no sequence similarity phase separate,[11, 35] and the length and time scales relevant to these condensed phases are far beyond the atomic scale, LLPS is reminiscent of the two-dimensional phase separation that produces domains in lipid membranes and that provides a conceptual foundation for understanding biological membranes.[36] Coarse-grained molecular simulations have been shown to reproduce the equilibrium structure[37] and self-assembly of amphiphilic membranes,[38] and the equilibrium properties of membranes on length scales larger than the constituent lipids are consistent for different coarse-graining strategies.[39] We propose that they may also provide insight into the structure and dynamics of LLPS.

Proteins and polymers are often represented in coarse-grained simulations as chains of beads connected by springs.[40-42] Their weak binding sites are treated as attractive interactions between selected beads. A common model places the binding sites at the ends of the molecules forming so-called *telechelic* polymers.[43] Brownian dynamics simulations of telechelic polymers show that they behave differently from pure random coils even in dilute solution in that their radius of gyration decreases when their end-caps are attractive.[44] Spatial correlations in the polymers' conformations arise from the end-cap interactions, and the viscosity of the telechelic polymer solution is higher than that of a non-associating polymer solution. Coarse-grained Molecular dynamics simulations of telechelic polymers at melt densities show that they self-assemble into spherical or worm-like micelles.[45] However, the high density of the melt phase is not representative of biomolecular condensates, that are typically found at very low volume fraction *in vivo* and *in vitro*.[22] Telechelics with hydrophobic end-caps self-

assemble into micellar structures driven by the strong repulsion of the end-caps from the solvent[43], but IDPs are generally soluble and the FUS LC domain lacks large hydrophobic regions. Nguemaha *et al.* have studied the influence of RNA on the phase separation of IDPs by representing the molecules as spherical particles with anisotropic interactions.[46] The effects of the RNA on the IDPs are described as a combination of a steric hindrance to aggregation and an interaction-dependent enhancement. Because the chain connectivity of the molecules is not explicitly represented, the internal structure of the droplet phase and its dependence on the IDP molecular weight are inaccessible. Chatteraj *et al.* have used Langevin dynamics to explore the effects of polymer backbone flexibility and steric effects on the clustering of a model of membrane-bound nephrin, adaptor protein Nck1, and the actin-nucleating protein NWASP driven by interaction domains on the proteins.[42] The system contained around 36 polymers, and revealed a relation between the polymers' conformational flexibility and their ability to cluster. Steric repulsion of inert sites located at the termini of the molecules reduced the mean cluster size more than inert sites close to binding sites in the middle of the molecules. This effect was attributed to the terminal domains of the fluctuating polymers limiting access to the interior binding sites. Harmon *et al.* performed lattice Monte Carlo simulations[41] in which an IDP is a linear polymer with multiple distributed binding sites – *stickers* – separated by flexible chain regions – *linkers*. The interaction between the sticker and linker monomers with the solvent are varied to explore the effects of preferential solvation on their aggregation. Their simulations predict that the differential solvation energy in a mixture of four polymer types leads to structured droplets in which polymers more strongly repelled from the solvent are enclosed by those that prefer solvation.

Here, we consider the N-terminal, low-complexity domain of FUS that has been shown to undergo LLPS alone.[4, 20] FUS LC contains mainly uncharged residues and is enriched in glutamine, glycine, serine and tyrosine (QGSY, Fig. 1). It

exhibits a wide range of conformations that have no secondary structure in solution nor in the condensed phase.[19] We represent FUS LC as a soluble, telechelic polymer with *sticky* end-caps (Figure 1). The backbone and end-caps are *hydrophilic*, so that only the self-attraction of the end-caps drives the polymers to associate. We note that although the end-caps of the model polymers are sticky this does not imply that the corresponding FUS LC must have binding sites only at its terminii. The end-caps of the model polymers can represent binding sites distributed a certain distance apart within the body of a longer domain. The self-assembly of model FUS LC is studied as a function of concentration and molecular architecture using coarse-grained Dissipative Particle Dynamics (DPD) simulations.[47-49] DPD has been used to study many soft matter systems and we refer the reader to section 1 of the Supplementary Information for more details.

The simulations show that polymers with sufficiently sticky end-caps spontaneously aggregate into porous, fluid networks in which the end-caps reversibly bind at spatially-distributed junctions as the polymers undergo conformational fluctuations. The spatial separation of the connected junctions scales with the polymer backbone length as a self-avoiding random walk, and is independent of the end-cap affinity providing it is sufficiently large that the network phase is stable. The large fluctuations of the polymers in the network allow them to retain the conformational entropy of the dilute phase while gaining enthalpy from their transiently-binding end-caps, thereby lowering the free energy of the network below that of the dispersed phase. We propose that this provides a generic mechanism by which cells may regulate the formation and composition of BCs. Only IDPs whose binding site separation and affinity allow them to reversibly bind to each other in a network while retaining the high conformational entropy of the dispersed phase will condense into the same droplet. Post-translational modification of IDPs such as Tau[50] and weak interactions with chaperone proteins[51] modify their conformational ensemble. A cell could tune the

stability of their condensed phase by adjusting this ensemble to change the effective length or binding affinity. Additional proteins would be recruited to a droplet only if their conformational fluctuations and active binding sites are commensurate with those of the existing network.

RESULTS

We study a simplified model of an IDP such as the FUS LC (Fig. 1A) by representing it as a linear polymer with *sticky* end-caps (Fig. 1B). We do not attempt to reproduce the sequence specificity of FUS LC but construct a model that we believe captures the physical chemical nature of IDPs. The molecular architecture is described by the formula $E_M B_N E_M$ where N is the number of backbone beads of type B, which is varied to represent IDPs of different molecular weight, and each end-cap contains M beads of type E. Each backbone bead (B) corresponds to several amino acid residues, and the end-cap E beads represent weak, nonspecific binding domains. The aqueous solvent is represented by a single bead W. All beads have a size d_0, which is the range of the DPD forces and sets the length scale in the simulations. Table 1 lists the non-bonded interaction parameters, a_{ij} between bead types i and j, and the bond potential parameters used to connect beads into molecules. We emphasize that both the backbone and end-cap beads are hydrophilic so there is no hydrophobic repulsion from the solvent driving their aggregation. The attraction between the end-caps is quantified by a dimensionless binding affinity ϵ that is defined so that $\epsilon = 0$ corresponds to no affinity and $\epsilon = 1$ is a very strong affinity. Further details of the simulations and the definition of the binding affinity in terms of the DPD force field parameters are given in sections 1 - 3 of the Supporting Information.

Preliminary simulations showed that IDPs whose end-caps have $M < 4$ do not assemble into a condensed phase even for strongly attractive end-caps (data not

shown). All IDPs in this work therefore have end-caps with M=4 as shown in Fig. 1A, and are described by the formula $E_4B_NE_4$. The cross shape of the four end-cap beads is chosen so that they expose an approximately isotropic interaction surface. Hereafter, we refer to polymers $E_4B_NE_4$ with N backbone beads by the formula B_N for brevity. Early simulations showed that the large conformational fluctuations of completely flexible polymers concealed their binding sites within compact conformations and precluded aggregation, an effect reported previously in the literature.[42] Therefore, a bending stiffness is applied to the polymer backbone to represent the semi-flexible nature of IDPs without assuming any particular secondary structure (see Table 1).

Telechelic polymers spontaneously aggregate into fluid networks at low concentrations

We first describe the conditions under which polymers of type B_{16} spontaneously aggregate into networks as their concentration, backbone length and end-cap affinity are varied. Figure 2 shows snapshots from simulations of 634 polymers of type B_{16} in a simulation box of size $(48d_0)^3$ with the affinity increasing from left to right and top to bottom. Unless otherwise stated, this system size is used for all the results presented. Polymers with zero end-cap affinity ($\varepsilon = 0$, Fig. 2, top left) are always dispersed in the solvent. Those with low affinity ($\varepsilon = 0.68$, Fig 2, top right, and Supplementary Movie 1) form transient clusters while those with higher affinities ($\varepsilon = 0.8$, Fig. 2, bottom left and Supplementary Movie 2, and $\varepsilon = 0.96$, Fig. 2, bottom right and Supplementary Movie 3) spontaneously assemble into connected networks in which the end-caps meet at *junctions* while a small number of polymers remain free in the solvent. Figure 2 shows that the junctions appear to have a somewhat regular distribution in space, but do not form a lattice structure. We quantify this observation in the next section. Similar behaviour is found for polymers of length B_8, B_{10}, B_{24}, B_{32} (see Fig. S1 and Supplementary Movies 4 and 5). No polymers in the length range studied with an end-cap affinity below $\varepsilon = 0.6$ were found to form networks. Henceforth, we refer

to affinities close to ε ~ 0.6 as *low*, values at or above ε ~ 0.8 as *high*, and values ε ~ 0.96 as *very high* with the understanding that these are qualitative designations only. They reflect observed differences in the formation and appearance of networks seen, for example, in Figures S1 - S4.

Visual inspection of the simulation snapshots shows that polymers continually join and leave a network, and it can break up and reform during a simulation, especially for lower affinities. This raises the question of which network to use for quantitative measurements. Condensed phases of IDPs in experiments are typically microns in size, while our largest simulated networks approach 50 nm. We find that the structural properties of simulated networks containing hundreds to thousands of polymers are independent of their size, which implies that such networks are a thermodynamic phase. In the remainder of this work, we report quantitative properties only for the single largest network in a simulation as it evolves in time. This is referred to as the *Largest Equilibrium Network* (LEN). The algorithm for identifying the LEN is described in section 4 of the Supporting Information.

Figure 3 shows that the LEN size increases linearly with the polymer concentration above a threshold that depends on the end-cap affinity. This threshold results from distinct effects of the end-cap affinity on the conformational ensemble of dispersed polymers. Polymers with low affinity (ε = 0.68) have large conformational fluctuations that prevent them aggregating until their concentration confines their end-caps sufficiently to bind to each other. Polymers with very high affinity (ε = 0.96) form small, micelle-like aggregates in which their end-caps are surrounded by their backbones (Fig. S2 and Supplementary Movies 6 and 7). This state persists until the concentration is sufficiently high that the micelle-like structures unfold and merge into a network. We note again here that unlike amphiphilic micelles, there is no hydrophobic repulsion driving the polymers to aggregate. The micelle-like structures result from the strong

attraction of the end-caps for each other.

Polymers with strong end-cap affinity spontaneously condense into a network even at very low concentrations. For example, the LEN composed of B_{16} polymers with high-affinity end-caps ($\varepsilon = 0.8$) in a system with a concentration 0.002 contains almost all of the available polymers (622 polymers out of 634) with fewer than 2% dispersed in the bulk. Fewer than 11% remain dispersed for all higher concentrations and backbone lengths with this affinity. Reducing the affinity delays the appearance of a stable LEN until the concentration has exceeded a threshold, but even then many polymers remain dispersed in the bulk solvent. We find that 40% of polymers B_8, and 90% of polymers B_{10}, B_{16}, B_{24}, B_{32} with low-affinity end-caps ($\varepsilon = 0.68$) are dispersed in the bulk solvent at a concentration of 0.002. Around 10% remain dispersed for all backbone lengths B_8, B_{10}, B_{16}, B_{24}, B_{32} studied at the highest concentration (0.008).

Junction separation in the network is selected by the polymer length

Figure 2 and Figure S1 show that junctions appear rather uniformly distributed in space. We quantify this observation by defining the distance between connected junctions as the mean value of the end-to-end length of all polymers whose end-caps reside on the junctions. This quantity is averaged over all pairwise-connected junctions in the LEN to give the *Mean Junction Separation* L_{ee}. Close inspection of the networks reveals that some polymers have both of their end-caps residing on the same junction (see Figs. S3, S4 and Supplementary Movies 8 and 9). We exclude these ring-like conformations from the measurements of L_{ee} because they do not contribute towards the junction separation (see section 5 of the Supporting Information for more details).

Figure 4 shows the variation of L_{ee} with polymer concentration for networks composed of polymers B_8 to B_{32} with very high affinity ($\varepsilon = 0.96$), high-affinity ($\varepsilon = 0.8$) and low-affinity ($\varepsilon = 0.68$) end-caps. Three interesting observations can be

made from this data. First, the mean junction separation L_{ee} in the LEN is independent of polymer concentration (above a minimum value at which a stable LEN is formed). The shape of the networks quantified in Fig. 4 varies from small, nearly-spherical droplets to extended networks that span the periodic boundaries of the simulation box (*cp.* Fig. 2). But the internal structure, as measured by L_{ee}, is the same for all network shapes. We have ensured that the networks are equilibrated by comparing the values of L_{ee} averaged over widely-spaced times in the simulations (see section 6 of the Supporting Information and Figures S7 and S8). We have also confirmed that L_{ee} is independent of the simulation box size by performing simulations in a larger box $(64d_0)^3$ (see section 7 of the Supporting Information and Fig. S9).

Second, L_{ee} is almost independent of the end-cap affinity from the lowest value ($\varepsilon = 0.68$) to the highest value studied ($\varepsilon = 0.96$) as shown by the near superposition of the curves in Fig. 4 for polymers with the same backbone length but different affinities. As no networks were observed for polymers with affinities below $\varepsilon = 0.68$, it appears that as soon as the affinity/backbone length are compatible with a stable network, the spatial structure of the network remains unchanged for all higher affinities. This indicates that the LEN is a thermodynamic phase whose macroscopic properties are independent of its size and shape. We have verified that the network is fluid by performing a simulated Fluorescence Recovery after Photobleaching Experiment (FRAP).[52] A network of 1215 B_{16} polymers was allowed to form and equilibrate. The fluorescence bleaching effect in a FRAP experiment is represented in the simulations by assigning a different display colour to the end-cap beads of all polymers in one half of the network (yellow beads in Fig. S5). The labelled polymers are subsequently observed to diffuse through the network. Networks of B_8 and B_{24} polymers show similar behaviour as do networks of polymers with lower affinity (data not shown).

Third, the fraction of polymers in the LEN that adopt ring conformations decreases with increasing polymer concentration to an asymptotic value that is independent of the concentration. The asymptotic value increases with increasing end-cap affinity and decreasing polymer length (Fig. S6). It approaches about 10% for polymers with low affinity ($\varepsilon = 0.68$) end-caps and 20% for those with high affinity ($\varepsilon = 0.8$) end-caps. Polymers with the highest affinity studied ($\varepsilon = 0.96$) have the largest fraction of ring conformations, above 50%, for low concentrations of polymers shorter than B_{24} (see top curves in Fig. S6). These polymers form *micelle-like* structures in the dispersed phase as mentioned before (see Fig. S2 and Supplementary Movie 6) and maintain ring conformations within the network phase (Fig. S3). As the backbone length increases to B_{32} and B_{48}, the networks composed of the highest affinity ($\varepsilon = 0.96$) polymers start to resemble those of low-affinity polymers once their concentration exceeds 0.002, and less than 15% adopt ring conformations in the networks. This occurs because a polymer's conformational entropy increases with backbone length and opposes the ring-like conformations. We conclude that ring conformations are present in the LEN at all concentrations studied, but their proportion in the network decreases with increasing network size towards an asymptotic value that depends on the end-cap affinity, but only weakly on polymer length. The persistence of these rings in networks at higher polymer concentrations suggests that they are not driving the dispersed polymers into the network phase. This distinguishes the simulated networks from the theoretical transition between dispersed ring-like polymers and a network phase analysed by Semenov and Cates.[53]

Scaling relation of junction separation with backbone length

The near superposition of the curves of L_{ee} in Figure 4 for polymers with the same backbone length N but different concentrations and affinities suggests that the mean junction separation L_{ee} may scale with the polymer backbone length. Figure 5 shows that L_{ee} / N^{ν}, where $\nu = 0.6$ is the Flory exponent for self-avoiding

random walks (SAW), is independent of the polymer length for all three affinities studied from weak ($\varepsilon = 0.68$) to very strong ($\varepsilon = 0.96$). The prefactor of the scaling relation shows a weak affinity dependence as the curve moves down the ordinate axis with decreasing affinity. This scaling is a generic property of the networks at equilibrium, and we have checked that the junction separation is independent of time for both high (Fig. S7) and low (Fig. S8) end-cap affinities. We note here that all quantitative results are sampled from equilibrium states of the network after discarding at least the first million time-steps (see section 6 of the Supporting Information for a discussion of statistical errors.)

The distribution of polymers at junctions depends on end-cap affinity

We refer to the number of polymers whose end-caps meet at a given junction as the *junction mass*. Figure 6 shows that the mean junction mass in a network of polymers with backbone length B_{16} and shorter is approximately independent of concentration for polymers with high affinity ($\varepsilon = 0.8$) end-caps. The junction mass shows a weak increase with concentration for longer polymers with the same affinity. Polymers with low affinity ($\varepsilon = 0.68$) end-caps show a weak increase in the junction mass for all backbone lengths. The asymptotic value of the junction mass increases with decreasing backbone length for both affinities. For fixed backbone length, the junction mass is larger for higher-affinity polymers than for the lower-affinity ones. We conclude that increasing the polymer concentration at fixed backbone length leads to larger networks with the same internal structure (as measured by L_{ee} and mean junction mass) rather than greatly increasing the number of polymers spanning the junctions of the network.

The distribution of the junction mass throughout the network is very different for polymers with high and low affinity end-caps. Figure 7A shows that the junction mass distribution for high-affinity networks ($\varepsilon = 0.8$) is very broad, spanning the range from 3 - 30 polymers/junction, and approximately normal. The two histograms are sampled from widely-separated times in the simulation and show

that the mass distribution is invariant in time although polymers diffuse through the network (as confirmed by the FRAP simulation, Fig. S5). The enhancement in the number of junctions with fewer than 5 polymers arises because junctions near the surface of the network are largely surrounded by solvent and therefore have fewer polymers meeting at them than those in the network's core. By contrast, Figure 7B shows that the junction mass distribution is exponential for low-affinity networks and rarely has more than 10 polymers/junction. The weak affinity makes it less likely for many polymers to bind at the junctions of the network, but the network structure is stable and invariant in time as seen in the two histograms from different times.

DISCUSSION

Liquid-liquid phase separation of intrinsically-disordered proteins into biomolecular condensates is an important means by which cells spatiotemporally segregate their biochemical functions.[3] The disordered proteins typically have little or no secondary structure and exhibit a large ensemble of conformations.[54] In spite of an abundance of experimental examples,[18] the structural organisation of IDPs in the condensed phase is still obscure, although experiments on FUS,[4, 19, 20] LAF1[22] and Sup35[23] reveal that they form a fluid, mesh-like network in which the proteins are highly disordered. These results are difficult to describe within the usual Flory Huggins theory of polymer solutions,[25] which has prompted modifications of the theory.[14] This theory assumes that: 1) the enthalpic term involving interactions between the monomers and solvent favours segregation of the polymers, and, 2) the ideal-chain *translational* entropy drives the polymers to mix with the solvent. The low density within experimental condensates suggests that the IDPs do not interact strongly at the monomer-monomer scale, and their translational entropy is low compared to their conformational fluctuations.

We have used coarse-grained simulations to quantify the structure of the

condensed phase of a model intrinsically-disordered protein exemplified by the low-complexity domain of FUS. The IDPs are represented as semi-flexible polymers with sticky end-caps in a good solvent. The polymers condense into a network whose structural properties qualitatively reproduce experimental features of biomolecular condensates, and make quantitative predictions relating the condensate's structure to the molecular properties of the IDP. The network is fluid and has a low internal polymer density as seen in experiments.[22] The polymers exhibit large conformational fluctuations within the network[19] even as their end-caps reversibly bind to each other at junctions throughout the network volume as found in experiments on FUS LC.[20] The inter-junction separation is predicted to scale with the polymer backbone length with the Flory exponent for a self-avoiding walk *independently* of the binding site affinity and polymer concentration as long as these are in the regime where the network phase is stable. This prediction could be tested in experiments that determine the mesh size of the condensed phase for proteins with binding sites at different separations along the backbone. We note that this scaling behaviour is distinct from that of hydrogels, for which the cross-link separation *decreases* with increasing concentration due to compression of the *permanently* cross-linked polymers.[55] Our results imply that the low protein density within phase separated droplets is a prerequisite for their stability. The high porosity of the droplets allows the polymers to retain their large conformational fluctuations, and therefore their conformational entropy, while their end-caps move between the junctions. The gain in enthalpy from the weak, reversible binding is then sufficient to reduce the droplet's free energy below that of the dispersed phase.

If IDPs are generically driven to phase separate as our model suggests, how does a cell control their phase? Why do all IDPs in a region not condense into a single multicomponent droplet? Our results suggest that the answer to both questions lies in the sensitivity of the network's stability to the binding site affinity and separation of the constituent proteins. The conformational ensemble of RNA-

binding proteins is known to change when the protein is phosphorylated,[50] and is important for the formation and control of RNA granules.[51, 56] Many IDPs have multiple weak interaction sites and post-translational modification sites. Activating these sites or the binding of chaperone proteins may change the effective strength or separation of interaction sites and therefore the conformational ensemble of the protein.[57] If the binding site affinity is sufficiently strong at a given separation the network will be stable, but if the effective separation increases, or the affinity decreases, the network will dissolve. Because distinct interactions between binding sites on an IDP[14, 19] are encoded in the amino acid sequence,[13] a cell has a combinatorial mechanism to regulate their assembly into biomolecular condensates by activating or deactivating these binding sites.

The network's sensitivity to the conformational fluctuations of its constituent IDPs may also regulate its composition. Multicomponent biomolecular condensates have been proposed to be contain two classes of constituent referred to as scaffolds and clients.[2, 18] Scaffold proteins are multivalent, flexible molecules that form the core network of a BC. Biomolecular condensates composed of one or more scaffold IDPs could act as *filters* or *enhancers* of biochemical reactions by recruiting only client proteins whose conformational fluctuations/binding site affinity are commensurate with the existing network structure. The residence times of the client proteins will reflect the amount by which their conformational fluctuations deviate from those of the scaffold protein. It has been found that FUS is recruited into disordered aggregates formed by the mutant Huntingtin protein Htt-Q103 by a process that requires the presence of its N-terminal disordered region but not its RNA binding domain.[58] This is consistent with our hypothesis that IDPs that retain their conformational fluctuations on entering an existing condensate will be recruited, while those that incur an entropic cost due to incommensurate length, will be excluded. This hypothesis could be tested in experiments that reposition (or activate/deactivate) binding sites along IDPs, thereby modulating their conformational fluctuations relative to those of the

scaffold proteins. Opto-genetic experiments[59] that attach an inert linker segment to an IDP known to phase separate could be used to modify the phase diagram of the protein. We intend to test these hypotheses in future simulations to map out the phase diagram of networks composed of a mixture of telechelic polymers of different backbone lengths and binding site distributions.

Our model also suggests that the irreversible aggregation of IDPs may be assisted by mutation-enhanced changes in their conformational ensemble within the network.[60] Experiments on the Alzheimer's disease-related protein tau have found that phosphorylation increases its end-to-end length,[61] and that hyperphosphorylation opens up its hexapeptide repeats causing an amyloidogenic change in its conformational ensemble.[50] A single point mutation to α-Synuclein only four residues apart causes a 400-fold drop in binding affinity.[62] This sensitivity to local changes of an IDP's structure that is already flexible is surprising. Our results suggest it results from the strong requirement that an IDP's binding sites reversibly bind while the protein fluctuates within its conformational ensemble. Small changes to an IDP's ensemble within the network can bring additional binding sites within range that lead them to bind more tightly and eventually become irreversibly bound.[16, 63] This opens up a new route for therapeutic intervention against chronic neurodegenerative diseases.[64] The conformational ensemble of a disease-prone IDP could be manipulated by engineering additional interaction sites into an IDP, by adding a disulphide bond to α Synuclein[57] or genetically modifying cells to produce IDPs with alternative PTM sites,[65] additional covalent or non-covalent interactions, or biochemically-inert linker domains. If the modified conformational fluctuations move the relevant binding sites beyond range of each other, IDPs in the condensed phase would be resistant to aberrant liquid-solid transitions.

MATERIALS AND METHODS

Details of the Dissipative Particle Dynamics technique can be found in the associated Supporting Information. Snapshots and movies of the simulated networks were produced using the open-source VMD software from the University of Illinois Urbana Champaign (http://www.ks.uiuc.edu/Research/vmd/). Figure 1 was created with Biorender (https://app.biorender.com). The analysis was performed using custom python code written by the authors, and included algorithms from the open source library scikit-learn (https://scikit-learn.org/stable/index.html) as described in the Supporting Information. The executable DPD code and simulation data sets are available on reasonable request to the corresponding author.

ACKNOWLEDGEMENTS

The authors express their gratitude to W. Pezeshkian for many interesting discussions and for the script to export simulation snapshot files in VMD format. This study was supported by funding to the Blue Brain Project, a research centre of the École polytechnique fédérale de Lausanne (EPFL), from the Swiss government's ETH Board of the Swiss Federal Institutes of Technology. The authors gratefully acknowledge computer time provided by the Blue Brain Project and Swiss National Supercomputing Centre and the Abacus 2.0 Super-Computing cluster at the University of Southern Denmark.

SUPPORTING INFORMATION

The Supporting Information includes the following:

Technical details of the simulations and extra results for networks of polymers with a range of backbone lengths and end-cap affinities; we perform a simulated Fluorescence Recovery after Photobleaching

experiment to demonstrate that the network is fluid; and verify the equilibrium state of the networks by comparing their time and system size dependence.

Movie 1 Initial stage of the aggregation of 634 polymers B_{16} with low affinity $\varepsilon = 0.68$.

Movie 2 Initial stage of the aggregation of 634 polymers B_{16} with high affinity $\varepsilon = 0.8$.

Movie 3 Initial stage of the aggregation of 634 polymers B_{16} with very high affinity $\varepsilon = 0.96$.

Movie 4 Initial stage of the aggregation of 1251 polymers B_8 with high affinity $\varepsilon = 0.8$.

Movie 5 Initial stage of the aggregation of 1180 polymers B_{24} with high affinity $\varepsilon = 0.8$.

Movie 6 Dilute phase of 326 polymers B_8 with very high affinity $\varepsilon = 0.96$ showing small, micelle-like structures.

Movie 7 Dilute phase of 324 polymers B_{16} with very high affinity $\varepsilon = 0.96$ showing loosely-connected, small droplets.

Movie 8 Initial stage of the aggregation of 1251 polymers B_8 with very high affinity $\varepsilon = 0.96$.

Movie 9 Initial stage of the aggregation of 624 polymers B_{24} with very high affinity $\varepsilon = 0.96$.

AUTHOR CONTRIBUTIONS

Corresponding author

julian.shillcock@epfl.ch

ORCID

Julian C. Shillcock: 0000-0002-7887-735X

JCS and JHI conceived the study; JCS performed the simulations; MB and EC wrote the analysis code. MB, EC, and JCS performed the data analysis, and all authors discussed the results; JCS and JHI wrote the manuscript and all authors commented on and revised the manuscript.

CONFLICT OF INTEREST

The authors declare no competing financial interests.

REFERENCES

1. Boeynaems, S.; Alberti, S.; Fawzi, N. L.; Mittag, T.; Polymenidou, M.; Rousseau, F.; Schymkowitz, J.; Shorter, J.; Wolozin, B.; Bosch, L. V. D.; Tompa, P.; Fuxreiter, M., Protein Phase Separation: A New Phase in Cell Biology. *Trends Cell Biology* **2018,** *28*, 420-435.

2. Banani, S. F.; Lee, H. O.; Hyman, A. A.; Rosen, M. K., Biomolecular Condensates: Organizers of Cellular Biochemistry. *Nature Rev. Mol. Cell Biol.* **2017,** *18*, 285-298.

3. Holehouse, A. S.; Pappu, R. V., Functional Implications of Intracellular Phase Transitions. *Biochemistry* **2018,** *57*, 2415-2423.

4. Patel, A.; Lee, H. O.; Jawerth, L.; Maharana, S.; Jahnel, M.; Hein, M. Y.; Stoynov, S.; Mahamid, J.; Saha, S.; Franzmann, T. M.; Pozniakovski, A.; Poser, I.; Maghelli, N.; Royer, L. A.; Weigert, M.; Myers, E. W.; Grill, S.; Drechsel, D.; Hyman, A. A.; Alberti, S., A Liquid-to-Solid Phase Transition of the ALS Protein FUS Accelerated By Disease Mutation. *Cell* **2015,** *162*, 1066-1077.

5. Chong, P. A.; Forman-Kay, J. D., Liquid-Liquid Phase Separation in Cellular Signalling Systems. *Curr. Op. Struct. Biol.* **2016,** *41*, 180-186.

6. Li, P.; Banjade, S.; Cheng, H.-C.; Kim, S.; Chen, B.; Guo, L.; Llaguno, M.; Hollingsworth, J. V.; King, D. S.; Banani, S. F.; Russo, P. S.; Jiang, Q.-X.; Nixon, B. T.; Rosen, M. K., Phase Transitions in the Assembly of Multivalent Signalling Proteins. *Nature* **2012,** *483*, 336-341.

7. Su, X.; Ditlev, J. A.; Hui, E.; Xing, W.; Banjade, S.; Okrut, J.; King, D. S.; Taunton, J.; Rosen, M. K.; Vale, R. D., Phase Separation of Signaling Molecules Promotes T Cell Receptor Signal Transduction. *Science* **2016,** *352*, 595-599.

8. Zeng, M.; Shang, Y.; Araki, Y.; Guo, T.; Huganir, R. L.; Zhang, M., Phase Transition in Postsynaptic Densities Underlies Formation of Synaptic Complexes and Synaptic Plasticity. *Cell* **2016,** *166*, 1163-1175.

9. Shin, Y.; Chang, Y.-C.; Lee, D. S. W.; Berry, J.; Sanders, D. W.; Ronceray, P.; Wingreen, N. S.; Haataja, M.; Brangwynne, C. P., Liquid Nuclear Condensates Mechanically Sense and Restructure the Genome. *Cell* **2018,** *175*, 1481-1491.

10. Aguzzi, A.; Altmeyer, M., Phase Separation: Linking Cellular Compartmentalization to Disease. *Trends Cell Biology* **2016,** *26*, 547-558.

11. Brown, C. J.; Johnson, A. K.; Dunker, A. K.; Daughdrill, G. W., Evolution and Disorder. *Current Opinion in Structural Biology* **2011,** *21*, 441-446.

12. Oldfield, C. J.; Dunker, A. K., Intrinsically Disordered Proteins and Intrinsically Disordered Protein Regions. *Annu. Rev. Biochem.* **2014,** *83*, 553-584.

13. Wang, J.; Choi, J.-M.; Holehouse, A. S.; Lee, H. O.; Zhang, X.; Jahnel, M.; Maharana, S.; Lemaitre, R.; Pozniakovsky, A.; Drechsel, D.; Poser, I.; Pappu, R. V.; Alberti, S.; Hyman, A. A., A Molecular Grammar Governing the Driving Forces for Phase Separation of Prion-Like RNA Binding Proteins. *Cell* **2018,** *174*, 688-699.

14. Brangwynne, C. P.; Tompa, P.; Pappu, R. V., Polymer Physics of Intracellular Phase Transitions. *Nature Physics* **2015,** *11*, 899-904.

15. Holehouse, A. S.; Pappu, R. V., Collapse Transitions of Proteins and the Interplay Among Backbone, Sidechain, and Solvent Interactions. *Annu. Rev. Biophys.* **2018,** *47*, 19-39.

16. Alberti, S.; Hyman, A. A., Are Aberrant Phase Transitions a Driver of Cellular Aging? *Bioessays* **2016,** *38*, 959-968.

17. Mitrea, D. M.; Chandra, B.; Ferrolino, M. C.; Gibbs, E. B.; Tolbert, M.; White, M. R.; Kriwacki, R. W., Methods for Physical Characterization of Phase-Separated Bodies and Membraneless Organelles. *J. Mol. Biol.* **2018,** *430*, 4773-4805.

18. Alberti, S.; Gladfelter, A.; Mittag, T., Considerations and Challenges in Studying Liquid-Liquid Phase Separation and Biomolecular Condensates. *Cell* **2019,** *176*, 419-434.

19. Murthy, A. C.; Dignon, G. L.; Kan, Y.; Zerze, G. H.; Parekh, S. H.; Mittal, J.; Fawzi, N. L., Molecular Interactions Underlying Liquid-Liquid Phase Separation of the FUS Low-Complexity Domain. *Nature Struct. Mol. Biol.* **2019,** *26*, 637-648.

20. Burke, K. A.; Janke, A. M.; Rhine, C. L.; Fawzi, N. L., Residue-by-Residue View of In Vitro FUS Granules that Bind the C-Terminal Domain of RNA Polymerase II. *Molecular Cell* **2015,** *60*, 231-241.

21. Brady, J. P.; Farber, P. J.; Sekhar, A.; Lin, Y.-H.; Huang, R.; Bah, A.; Nott, T. J.; Chan, H. S.; Baldwin, A. J.; Forman-Kay, J. D.; Kay, L. E., Structural and Hydrodynamic Properties of an Intrinsically Disordered Region of a Germ Cell-Specific Protein on Phase Separation. *PNAS* **2017,** *114*, E8194-E8203.

22. Wei, M.-T.; Elbaum-Garfinkle, S.; Holehouse, A. S.; Chen, C. C.-H.; Feric, M.; Arnold, C. B.; Priestley, R. D.; Pappu, R. V.; Brangwynne, C. P., Phase Behaviour of Disordered Proteins Underlying Low Density and High Permeability of Liquid Organelles. *Nature Chemistry* **2017,** *9*, 1118-1125.

23. Franzmann, T. M.; Jahnel, M.; Pozniakovsky, A.; Mahamid, J.; Holehouse, A. S.; Nüske, E.; Richter, D.; Baumeister, W.; Grill, S. W.; Pappu, R. V.; Hyman, A. A.; Alberti, S., Phase Separation of a Yeast Prion Protein Promotes Cellular Fitness. *Science* **2018,** *359*, eaao5654-1 eaao5654-8.

24. Wang, Y.; Lomakin, A.; Kanai, S.; Alex, R.; Benedek, G. B., Liquid-Liquid Phase Separation in Oligomeric Peptide Solutions. *Langmuir* **2017,** *33*, 7715-7721.

25. Rubinstein, M.; Colby, R. H., *Polymer Physics*. Oxford University Press: New York, 2003.

26. Stroberg, W.; Schnell, S., On the Origin of Non-Membrane-Bound Organelles, and Their Physiological Function. *J. Theor. Biol.* **2017,** *434*, 42-49.

27. Brangwynne, C. P.; Eckmann, C. R.; Courson, D. S.; Rybarska, A.; Hoege, C.; Gharakhani, J.; Jülicher, F.; Hyman, A. A., Germline P Granules are Liquid Droplets That Localize by Controlled Dissolution/Condensation. *Science* **2009,** *324*, 1729-1732.

28. Ruff, K. M.; Pappu, R. V.; Holehouse, A. S., Conformational Preferences and Phase Behaviour of Intrinsically Disordered Low Complexity Sequences: Insights from Multiscale Simulations. *Curr. Op. Struct. Biol.* **2019,** *56*, 1-10.

29. Rauscher, S.; Gapsys, V.; Gajda, M. J.; Zweckstetter, M.; Groot, B. L. d.; Grubmüller, H., Structural Ensembles of Intrinsically Disordered Proteins Depend Strongly on Force Field: A Comparison to Experiment. *J. Chem. Theory and Comp.* **2015,** *11*, 5513-5524.

30. Kang, H.; Luan, B.; Zhou, R., Glassy Dynamics in Mutant Huntingtin Proteins. *J. Chem. Phys.* **2018,** *149*, 072333-072341.

31. Balupuri, A.; Choi, K.-E.; Kang, N. S., Computational Insights into the Role of α-Strand/Sheet in Aggregation of α-Synuclein. *Scientific Reports* **2019,** *9*, 59-1 - 59-13.

32. Lyons, A. J.; Gandhi, N. S.; Mancera, R. L., Molecular Dynamics Simulation of the Phosphorylation-Induced Conformational Changes of a Tau Peptide Fragment. *Proteins* **2014,** *82*, 1907-1923.

33. Barz, B.; Liao, Q.; Strodel, B., Pathways of Amyloid-β Aggregation Depend on Oligomer Shape. *JACS* **2017,** *140*, 319-327.

34. Ramis, R.; Ortega-Castro, J.; Casasnovas, R.; Mariño, L.; Vilanova, B.; Adrover, M.; Frau, J., A Coarse-Grained Molecular Dynamics Approach to the Study of the Intrinsically Disordered Protein α-Synuclein. *J. Chem. Inf. Model.* **2019,** *59*, 1458-1471.

35. Daughdrill, G. W.; Narayanaswami, P.; Gilmore, S. H.; Belcyzk, A.; Brown, C. J., Dynamic Behavior of an Intrinsically Unstructured Linker Domain is Conserved in the Face of Negligible Amino Acid Sequence Conservation. *J. Mol. Evol.* **2007,** *65*, 277-288.

36. Hyman, A. A.; Brangwynne, C. P., Beyond Stereospecificity: Liquids and Mesoscale Organization of Cytoplasm. *Dev. Cell* **2011,** *21*, 14-16.

37. Shillcock, J. C.; Lipowsky, R., Equilibrium Structure and Lateral Stress Distribution of Amphiphilic Bilayers from Dissipative Particle Dynamics Simulations. *J. Chem. Phys.* **2002,** *117*, 5048-5061.

38. Shillcock, J. C., Spontaneous Vesicle Self-Assembly: A Mesoscopic View of Membrane Dynamics. *Langmuir* **2012,** *28*, 541-547.

39. Venturoli, M.; Sperotto, M. M.; Kranenburg, M.; Smit, B., Mesoscopic Models of Biological Membranes. *Physics Reports* **2006,** *437*, 1-54.

40. Dignon, G. L.; Zheng, W.; Kim, Y. C.; Best, R. B.; Mittal, J., Sequence Determinants of Protein Phase Behavior from a Coarse-Grained Model. *PLoS Computational Biology* **2018,** *14*, e1005941.

41. Harmon, T. S.; Holehouse, A. S.; Pappu, R. V., Differential Solvation of Intrinsically Disordered Linkers Drives the Formation of Spatially Organised Droplets in Ternary Systems of Linear Multivalent Proteins. *New. J. Physics* **2018,** *20*, 045002-045016.

42. Chatteraj, A.; Youngstrom, M.; Loew, L. M., The Interplay of Structural and Cellular Biophysics Controls Clustering of Multivalent Molecules. *Biophys. J.* **2019,** *116*, 560-572.

43. Arai, N., Structural Analysis of Telechelic Polymer Solution Using Dissipative Particle Dynamics Simulations. *Mol. Sim.* **2015,** *41*, 996-1001.

44. Xiao, C.; Heyes, D. M., Brownian Dynamics Simulations of Attractive Polymers in Solution. *J. Chem. Phys.* **2002,** *117*, 2377-2388.

45. Manassero, C.; Raos, G.; Allegra, G., Structure of Model Telechelic Polymer Melts by Computer Simulation. *J. Macromol. Sci. Part B: Physics* **2005,** *44*, 855-871.

46. Nguemaha, V.; Zhou, H.-X., Liquid-Liquid Phase Separation of Patchy Particles Illuminates Diverse Effects of Regulatory Components on Protein Droplet Formation. *Sci. Rep.* **2018,** *8*, 6728-6739.

47. Hoogerbrugge, P. J.; Koelman, J. M. V. A., Simulating Microscopic Hydrodynamic Phenomena with Dissipative Particle Dynamics. *Europhys. Lett.* **1992,** *19*, 155-160.

48. Espagnol, P.; Warren, P. B., Statistical Mechanics of Dissipative Particle Dynamics. *Europhysics Letters* **1995,** *30*, 191-196.

49. Groot, R. D.; Warren, P. B., Dissipative Particle Dynamics: Bridging the Gap Between Atomistic and Mesoscopic Simulations. *J. Chem. Phys.* **1997,** *107*, 4423-4435.

50. Zhu, S.; Shala, A.; Bezginov, A.; Sljoka, A.; Audette, G.; Wilson, D. J., Hyperphosphorylation of Intrinsically Disordered Tau Protein Induces an Amyloidogenic Shift in Its Conformational Ensemble. *PLoS One* **2015,** *10*, e0120416.

51. Wang, Z.; Zhang, H., Phase Separation, Transition, and Autophagic Degradation of Proteins in Development and Pathogenesis. *Trends Cell Biology* **2019,** *29*, 417-427.

52. Taylor, N. O.; Wei, M.-T.; Stone, H. A.; Brangwynne, C. P., Quantifying Dynamics in Phase-Separated Condensates Using Fluorescence Recovery After Photobleaching. *Biophys. J.* **2019,** *117*, 1285-1300.

53. Semenov, A. N.; Nyrkova, I. A.; Cates, M. E., Phase Equilibria in Solutions of Associating Telechelic Polymers: Rings vs Reversible Network. *Macromolecules* **1995,** *28*, 7879-7885.

54. Protter, D. S. W.; Rao, B. S.; Treeck, B. V.; Lin, Y.; Mizoue, L.; Rosen, M. K.; Parker, R., Intrinsically Disordered Regions Can Contribute Promiscuous Interactions to RNP Granule Assembly. *Cell Reports* **2018,** *22*, 1401-1412.

55. Flory, P. J., *Principles of Polymer Chemistry*. Cornell University Press: Ithaca, 1953.

56. Weber, S. C.; Brangwynne, C. P., Getting RNA and Protein in Phase. *Cell* **2012,** *149*, 1188-1191.

57. Carija, A.; Pinheiro, F.; Pujols, J.; Brás, I. C.; Lázaro, D. F.; Santambrogio, C.; Grandori, R.; Outeira, T. F.; Navarro, S.; Ventura, S., Biasing the α-Synuclein Conformational Ensemble Towards Compact States Abolishes Aggregation and Neurotoxicity. *Redox Biology* **2019,** *22*, 101135-101150.

58. Wear, M. P.; Kryndushkin, D.; O'Meally, R.; Sonnenberg, J. L.; Cole, R. N.; Shewmaker, F. P., Proteins with Intrinsically Disordered Domains Are Preferentially Recruited to Polyglutamine Aggregates. *PLoS One* **2015,** *10*, e0136362.

59. Shin, Y.; Berry, J.; Pannucci, N.; Haataja, M. P.; Toettcher, J. E.; Brangwynne, C. P., Spatiotemporal Control of Intracellular Phase Transitions Using Light-Activated OptoDroplets. *Cell* **2017,** *168*, 159-171.

60. Murakami, T.; Qamar, S.; Lin, J. Q.; Schierle, G. S. K.; Rees, E.; Miyashita, A.; Costa, A. R.; Dodd, R. B.; Chan, F. T. S.; Michel, C. H.; Kronenberg-Versteeg, D.; Li, Y.; Yang, S.-P.; Wakutani, Y.; Meadows, W.; Ferry, R. R.; Dong, L.; Tartaglia, G. G.; Favrin, G.; Lin, W.-L.; Dickson, D. W.; Zhen, M.; Ron, D.; Schmitt-Ulms, G.; Fraser, P. E.; Schneier, N. A.; Hlt, C.; Vendruscolo, M.; Kaminski, C. F.; George-Hyslop, P. S., ALS/FTD Mutation-Induced Phase Transition of FUS Liquid Droplets and Reversible Hydrogels into Irreversible Hydrogels Impairs RNP Granule Function. *Neuron* **2015,** *88*, 678-690.

61. Chin, A. F.; Toptygin, D.; Elam, W. A.; Schrank, T. P.; Hilser, V. J., Phosphorylation Increases Persistence Length and End-to-End Distance of a Segment of Tau Protein. *Biophys. J.* **2016,** *110*, 362-371.

62. Turk, F. E.; Genst, E. D.; Guilliams, T.; Fauvet, B.; Hejjaoui, M.; Trani, J. D.; Chiki, A.; Mittermaier, A.; Vendruscolo, M.; Lashuel, H. A.; Dobson, C. M., Exploring the Role of Post-Translational Modifications in Regulating α-Synuclein Interactions by Studying the Effects of Phosphorylation on Nanobody Binding. *Protein Science* **2018,** *27*, 1262-1274.

63. Peskett, T. R.; Rau, F.; O'Driscoll, J.; Patani, R.; Lowe, A. R.; Saibil, H. R., A Liquid To Solid Phase Transition Underlying Pathological Huntingtin Exon1 Aggregation. *Mol. Cell* **2018,** *70*, 588-601.

64. Maity, B. K.; Vishvakarma, V.; Surendran, D.; Rawat, A.; Das, A.; Pramanik, S.; Arfin, N.; Maiti, S., Spontaneous Fluctuations Can Guide Drug Design Strategies for Structurally Disordered Proteins. *Biochemistry* **2018,** *57*, 4206-4213.

65. Monahan, Z.; Ryan, V. H.; Janke, A. M.; Burke, K. A.; Rhoads, S. N.; Zerze, G. H.; O'Meally, R.; Dignon, G. L.; Conicella, A. E.; Zheng, W.; Best, R. B.; Cole, R. N.; Mittal, J.; Shewmaker, F.; Fawzi, N. L., Phosphorylation of the FUS Low-Complexity Domain Disrupts Phase Separation, Aggregation and Toxicity. *EMBO Journal* **2017,** *36*, 2951-2967.

TABLES

Bead Pair	a_{ij}
WW	25
BB	25
EE	a_{EE}
WB	23
WE	25
BE	25

Table 1 Non-bonded conservative interaction parameters a_{ij} for all bead types (in units of k_BT/d_0). The backbone (B) and end-cap (E) beads are hydrophilic, which represents a polymer in a good solvent, and the parameter a_{EE} is varied to modify the end-caps' binding affinity: smaller values of a_{EE} correspond to increased attraction between the E beads as described in the Supporting Information section 3. The reduced value of a_{WB} ensures that the polymer backbone remains solvated in the network phase. The dissipative force parameters are 4.5 for all bead pairs (in units of $\sqrt{m_0 k_B T/d_0^2}$). Beads are connected into polymers using Hookean bonds. Based on previous simulations of amphiphilic membranes (Shillcock, Lipowsky 2002), the bond potential constrains the bonds' mean length, and the same values, $k_2 = 128\ k_BT/d_0^2$ and $l_0 = d_0/2$, are used for all bonded beads (EE, EB, BB). Chain stiffness is imposed by a bending potential for all BBB triples along the backbone with bending constant $k_3 = 5\ k_BT$. Further details of the simulations are given in the Supporting Information sections 1 and 2.

FIGURES

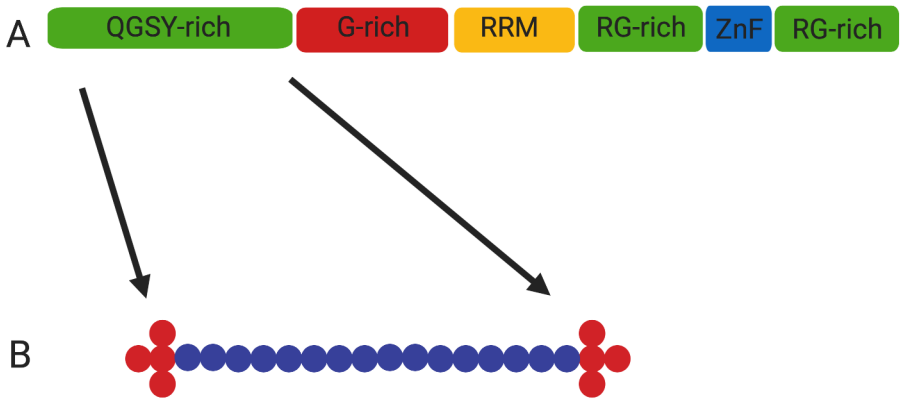

Figure 1 A) Domain sequence of the intrinsically-disordered protein FUS. The 526-residue FUS protein has intrinsically-disordered regions at the N and C termini that are mainly composed of uncharged residues and that contain weakly-binding interaction sites. Its internal domains contain an RNA recognition motif (RRM) and a zinc finger domain.

B) Cartoon of the polymer $E_4 B_{16} E_4$ that represents the disordered N-terminal domain of FUS in the simulations. We do not attempt to map the N-terminal residue sequence precisely in the model, but retain only its conformational flexibility and weak binding sites. The N-terminal disordered domain is reduced to a semi-flexible, linear polymer of hydrophilic backbone beads B with two hydrophilic, self-associating end-caps composed of beads E. The end-cap shape is chosen to increase its interaction volume. The backbone length is varied to represent disordered domains or proteins of different molecular weight and the end-cap affinity is varied to change their binding site affinity.

(Created with Biorender)

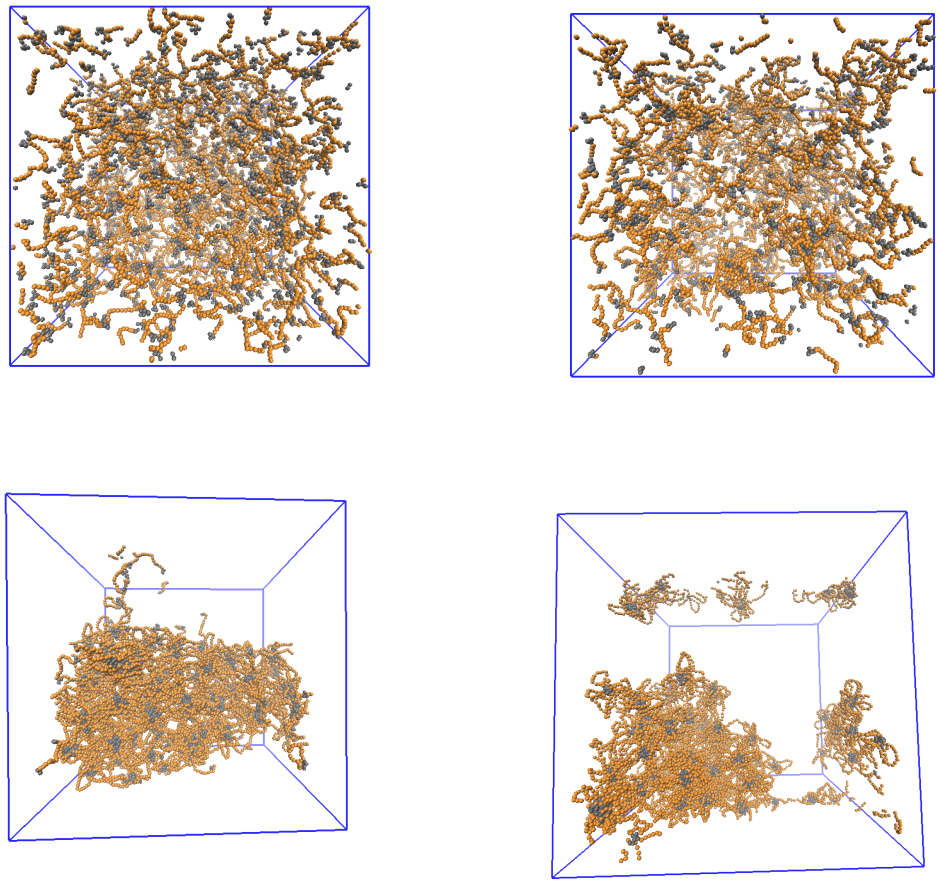

Figure 2 Snapshots of equilibrium configurations of 634 polymers of type $E_4B_{16}E_4$ in water (invisible for clarity in all snapshots) for four end-cap affinities. The end-caps (grey beads) possess (left to right, top to bottom): no affinity ($\varepsilon = 0$), weak affinity ($\varepsilon = 0.68$), strong affinity ($\varepsilon = 0.8$), very strong affinity ($\varepsilon = 0.96$). In the absence of end-cap affinity, the polymers are freely dispersed in the bulk solvent. For weak affinities, some polymers aggregate into small, transient clusters but a large network only forms at higher concentrations. For stronger affinities, most of the polymer condense into a single large network while a few remain dispersed in the bulk solvent. The apparently-disconnected pieces of network in the images appear because of the periodic boundary conditions of the simulation box.

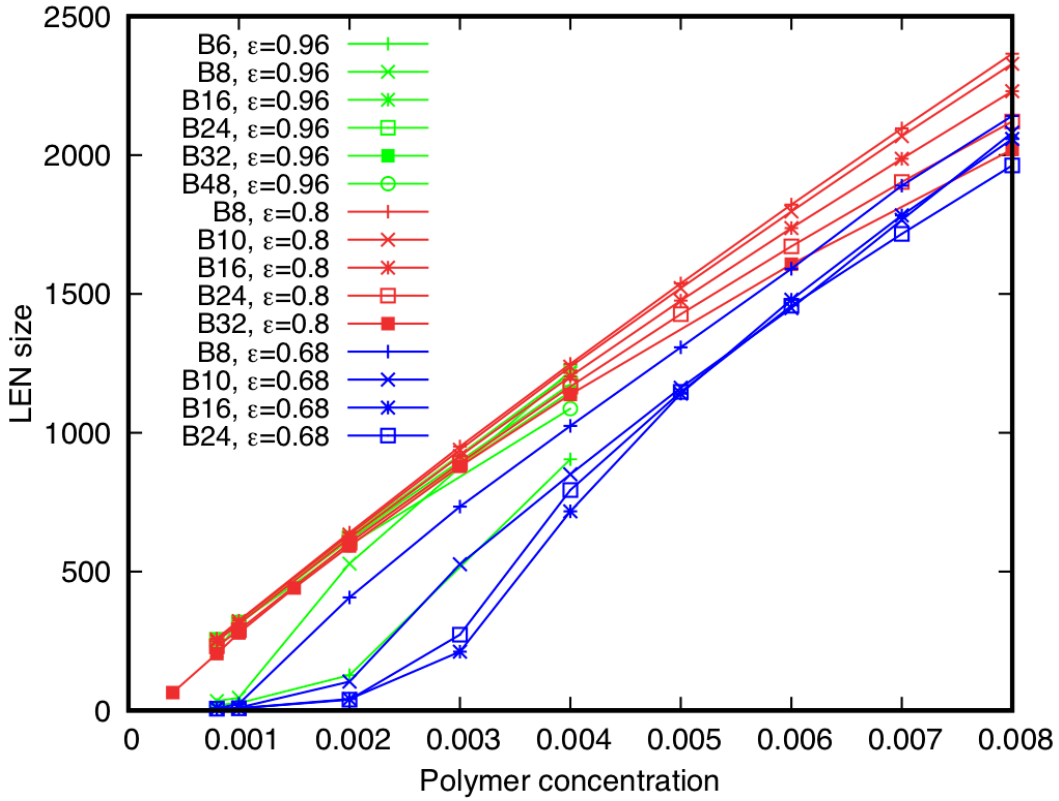

Figure 3 The number of $E_4B_NE_4$ polymers in the Largest Equilibrium Network as a function of the polymer concentration and backbone length (N) for three end-cap affinities ranging from weak to very strong (ε = 0.68, 0.8, 0.96). The network's size increases linearly with polymer concentration in all cases once the concentration exceeds an affinity-dependent threshold. Polymers with weak end-cap affinity (ε = 0.68) and lengths B_{10}, B_{16}, B_{24} do not aggregate at low concentrations because the low enthalpic gain of binding is insufficient to overcome their conformational entropy. Polymers with very high affinity (ε = 0.96) and short backbone length B_6 only aggregate above a threshold concentration because their high affinity causes them to form micelle-like structures at low concentrations that inhibits their end-caps meeting (see Fig. S2). Note that the highest affinity curves only reach polymer concentrations of 0.004.

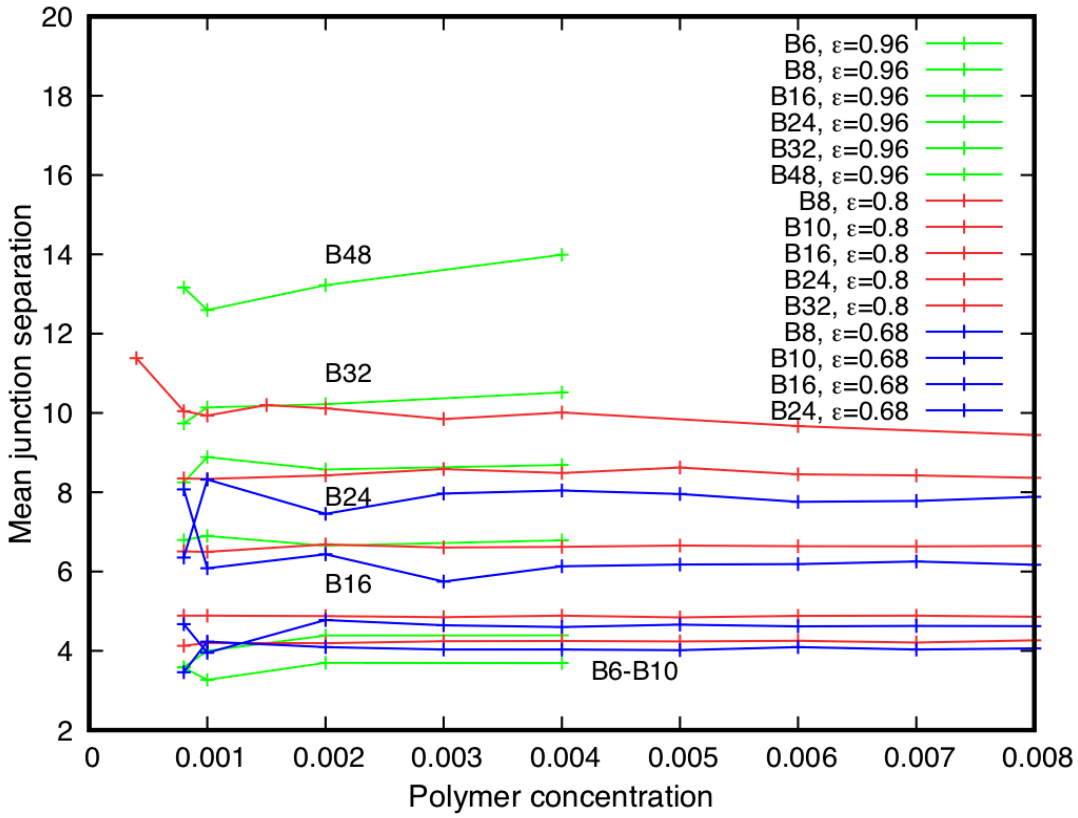

Figure 4 The major structural property of the Largest Equilibrium Network is the mean junction separation shown here as a function of polymer concentration for a range of backbone lengths and affinities. The junction separation in networks of polymers of all backbone lengths and end-cap affinities studied is independent of the polymer concentration above a minimum threshold concentration. The asymptotic value of the separation depends systematically on the backbone length, but only weakly on the end-cap affinity. The large fluctuations in the junction separation for polymers B_{16}, B_{24}, B_{32} at concentrations around 0.001 are due to the instability of the small networks.

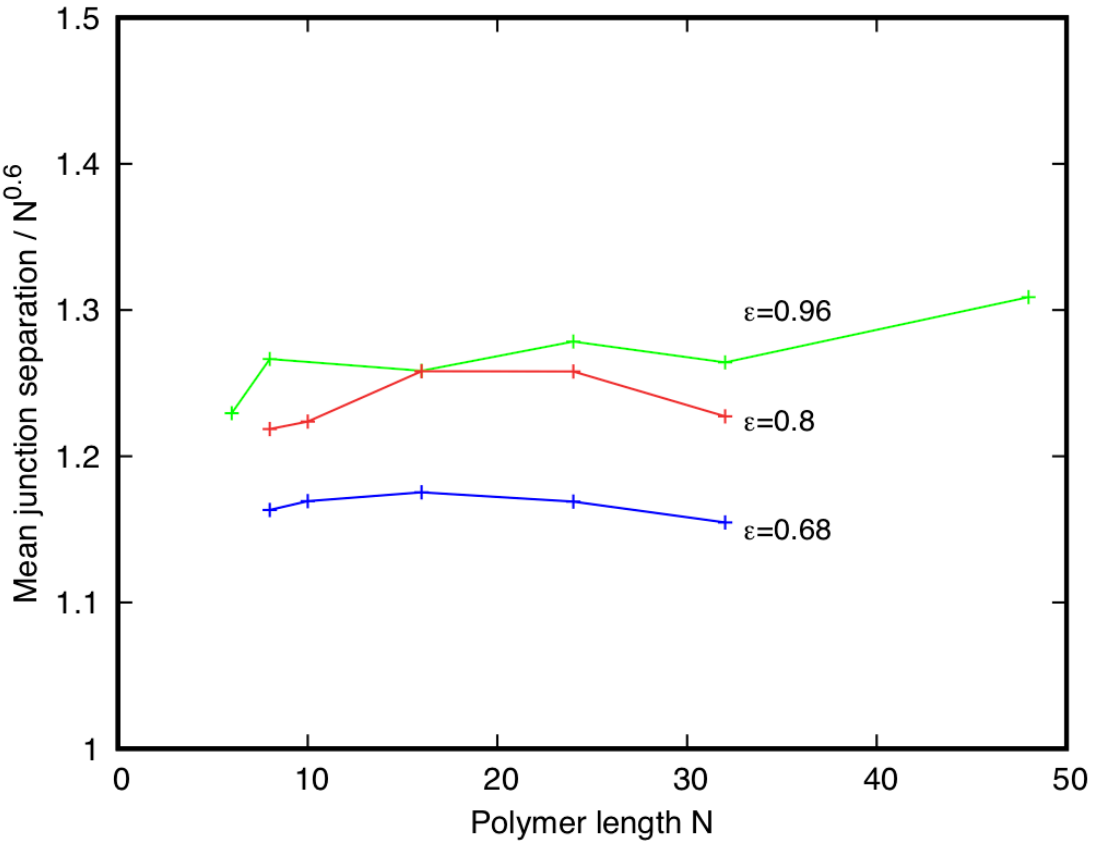

Figure 5 The mean junction separation in the Largest Equilibrium Network scales with the polymer backbone length as a self-avoiding random walk with Flory exponent 0.6 for all the end-cap affinities studied from weak (ε = 0.6), to strong (ε = 0.8), and very strong (ε = 0.96). A small affinity-dependent prefactor is evident by the displacement of the curves down the ordinate axis as the affinity decreases. The dependence of the junction separation on polymer length indicates that the networks are sufficiently porous that the polymer backbones fluctuate as self-avoiding polymers while their end-caps reversibly bind at the network junctions.

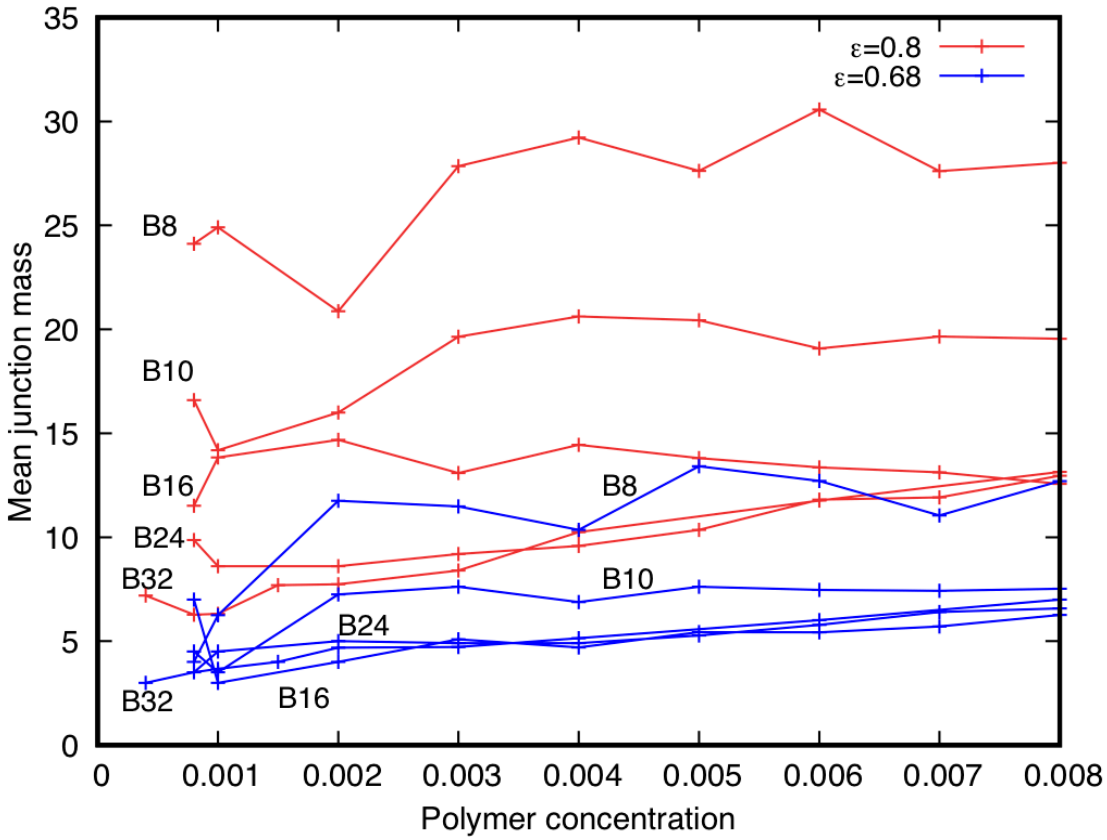

Figure 6 The mean number of polymers meeting at a junction (the junction *mass*) for strong (ε = 0.8, upper, red curves for polymers of length B_8, B_{10}, B_{16}, B_{24}, B_{32}) and weak (ε = 0.68, lower, blue curves for lengths B_8, B_{10}, B_{16}, B_{24}, B_{32}) end-cap affinities. The mean junction mass is independent of concentration for polymers with high affinity end-caps (ε = 0.8) whose backbone lengths are less than B_{16}, while it increases slowly with concentration towards a limiting value for B_{24} and B_{32} polymers. This limiting value is independent of the length for B_{16} and longer polymers, while it increases with decreasing backbone length for B_8, B_{10} polymers. Similar behaviour is seen for polymers with low-affinity end-caps (ε = 0.68), except that the limiting value of junction mass is smaller, and is reached for the wider range of polymer lengths B_{10}, B_{16}, B_{24}, B_{32}. Note that the spread of junction masses around the values shown here is very wide as shown in Fig. 7.

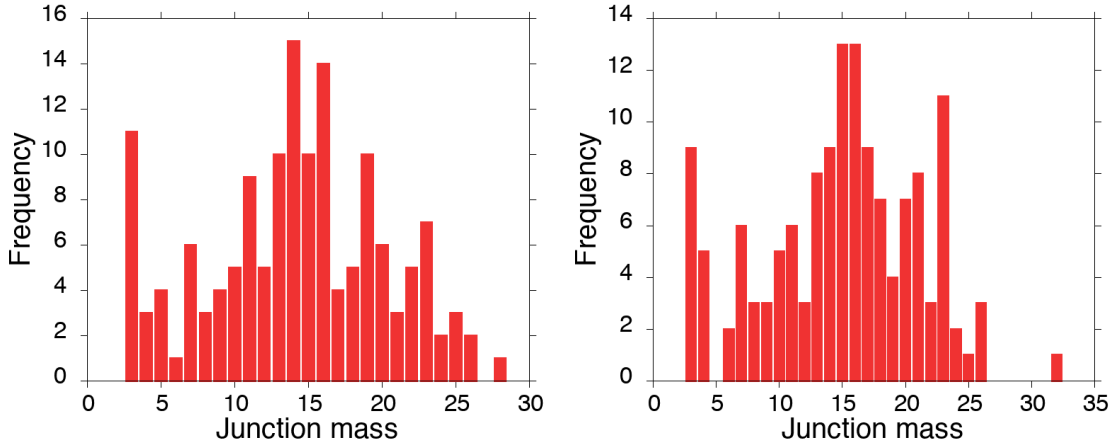

Fig. 7 A) Histograms of the relative frequency of the number of polymers meeting at a junction (the junction *mass*) for an equilibrated network of 1215 B_{16} polymers with high affinity (ε = 0.8) (left) and the same network 500,000 time-steps later (right). The mass distribution is broad and approximately normal with a mean value around 15 polymers/junction. The enhanced peak for junctions with 3-4 polymers is most likely due to junctions on the surface of the network being largely surrounded by solvent compared to those in the network interior. The variation in the histograms shows that the polymers redistribute among the junctions over time reflecting the fluidity of the network.

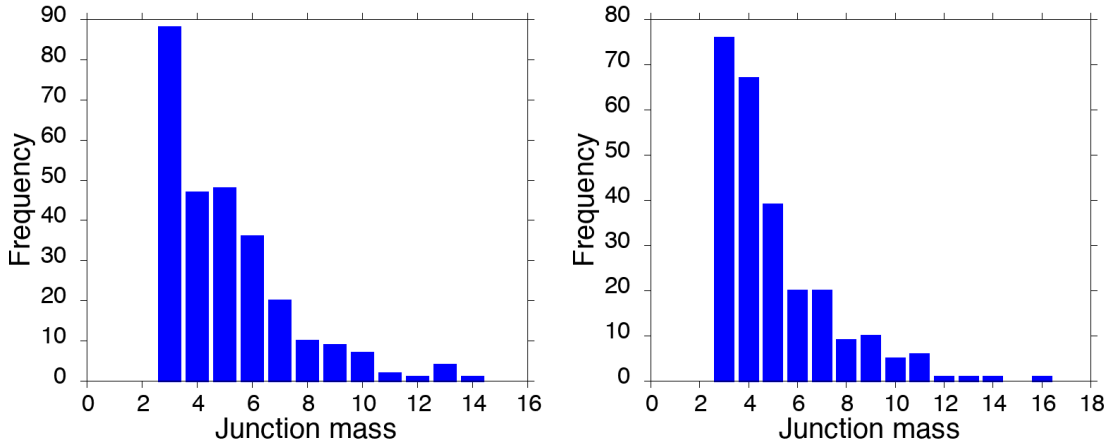

Fig. 7 B) Histograms of the relative frequency of the junction mass for an equilibrated network of 1215 B_{16} polymers with low affinity (ε = 0.68) (left) and the same network 500,000 time-steps later (right). In contrast to the high-affinity

case, the distribution is exponential with very few junctions having more than 10 polymers/junction. The variability in the histograms again reflects the fluid state of the network.